InP Shallow–Homojunction Solar Cells*

Christopher Keavney, Mark B. Spitzer, Stanley M. Vernon, Victor E. Haven
Spire Corporation

Godfrey Augustine
Georgia Institute of Technology

Summary

Indium phosphide solar cells with very thin n–type emitters have been made by both ion implantation and metalorganic chemical vapor deposition. Air mass zero efficiencies as high as 18.8% (NASA measurement) have been achieved. Although calculations show that, as is the case with GaAs, a heterostructure is expected to be required for the highest efficiencies attainable, the material properties of InP give the shallow–homojunction structure a greater potential than in the case of GaAs.

The best cells, which were those made by ion implantation, show open–circuit voltage (V_{oc}) of 873 mV, short–circuit current of 357 A/m^2 (35.7 mA/cm^2), and fill factor of 0.829. Improvements are anticipated in all three of these parameters. Internal quantum efficiency peaks at over 90% in the red end of the spectrum, but drops to 54% in the blue end. Other cells have achieved 74% in the blue end. Detailed modeling of the data indicates that a high front surface recombination velocity is responsible for the low blue response, that the carrier lifetime is high enough to allow good carrier collection from both the base and the emitter, and that the voltage is base–limited.

Introduction

Recently, much effort has been devoted to the study of InP solar cells for space applications. This work was sparked by the discovery that exposure to radiation, as in earth orbit, causes less damage to the photovoltaic performance of these cells than to that of GaAs or Si cells. Furthermore, the damage which is done can be annealed at a relatively low temperature [refs. 1 to 5].

The development of high–efficiency InP–based solar cell structures has proceeded quickly. Yamamoto [ref. 1] reported high–efficiency cells by a diffusion process and by liquid–phase epitaxy [ref. 6], while Coutts and Naseem [ref. 7] achieved remarkable results with a simple sputtered indium tin oxide heterojunction. Bothra [ref. 8] used another diffusion technique. Most recently, the highest–efficiency cells have been formed by metalorganic chemical vapor deposition [refs. 9 to 11]; these include p on n structures of 15.6% (AM0) efficiency [ref. 9] and the n on p structures described here of 18.8% [refs. 10 and 12]. Theory predicts an attainable beginning–of–life efficiency for this material nearly the same as that for GaAs. Because of the superior radiation resistance, this would correspond to a considerably higher end–of–life efficiency in typical space applications than any other known material.

*This work was performed under contract with the NASA Lewis Research Center.

Experimental

High–efficiency cells were made by metalorganic chemical vapor deposition (MOCVD), by ion implantation, and by a combination of the two techniques.

MOCVD cells were grown on heavily–doped p–type substrates ($4 \times 10^{24}m^{-3}$ [$4 \times 10^{18}cm^{-3}$], 2° off 100 orientation) and consisted of three layers: a buffer layer 0.5 μm thick, doped p–type to $4 \times 10^{24}m^{-3}$, a p–type base layer 3μm thick doped to approximately $2 \times 10^{22}m^{-3}$ ($2 \times 10^{16}cm^{-3}$), and an n–type emitter layer, doped to $10^{24}m^{-3}$ ($10^{18}cm^{-3}$) or higher, which varied in thickness. Growth was carried out in a SPI–MO CVD™ 450 reactor from tri–methylindium and phosphine. The growth conditions were as follows: 10 KPa (0.1 atm) pressure, 873–923 K temperature (600–650°C), P/In molar ratio of 80–400, and growth rate of 0.28–0.42 nm/s (1–1.5 μm/hour). SiH_4 and dimethylzinc were used as dopant sources.

For emitter thicknesses less than 100 nm, anodic oxidation was used to adjust the emitter thickness after epitaxy, as was done for GaAs cells by Fan, Bozler and Chapman [ref. 13]. The procedure of Robach et al. [ref. 14], using a dilute solution of phosphoric acid, was followed. An oxide of very uniform and controllable thickness could be formed in this manner, and cells with emitter thicknesses as small as 20 nm were successfully made.

Ion–implanted cells were formed from lightly doped ($2 \times 10^{22}m^{-3}$ [$2 \times 10^{16}cm^{-3}$]) p–type wafers.The wafers were implanted with an n–type dopant (Si, Se, or S) and then annealed at 1023 K (750°C) in a hydrogen atmosphere containing 2% PH_3. The substrate, in this structure, forms an active part of the cell.

The effects of implantation dose and energy were observed. Surface preparation was also found to be important; wafers chemically polished before implantation gave much better results than wafers implanted as received from the vendor; the latter showed some pitting during the anneal and gave low open–circuit voltages.

Hybrid cells were made by growing the buffer and base layers by MOCVD as described above, and then forming the emitter by ion implantation. This combination has yielded the highest efficiencies to date, because it combines the advantages of both techniques.

Both implanted and CVD cells were metallized as follows: 50 nm each of Zn and Au–10% Zn alloy were evaporated onto the back, then annealed at 723 K (450°C) for 60 s in a strip heater. 50 nm Pd and 500 nm Ag were evaporated after the anneal. The front contacts were Au:Ge–Ag or Cr–Au–Ag, with 2 μm of Ag, patterned by liftoff. The cells were mesa etched to 0.25 cm^2 final area, and a ZnS/MgF_2 antireflection coating was applied. Cells were tested under simulated AM0 conditions (1372 W/m^2) at 298 K (25°C), both at Spire and at NASA Lewis Research Center.

Results

Ion Implantation

Figure 1 shows the spectral response of three cells made by silicon implantation at three ion beam accelerating potentials. The dramatic increase in blue response with decreasing energy demonstrates the importance of thin junctions, a subject which is discussed at greater length in the modeling

section below. Table 1 gives the corresponding cell performance. The short–circuit currents reported for the 5 KV silicon implants are higher than those of any of the epixatial cells below; the 5 KV implant was incorporated into the hybrid cells which achieved 18.8%.

Anodic oxidation was used to examine the doping profile of three cells by differential Hall effect measurements; the results are seen in figure 2. The cells were repeatedly anodized to 10 V in the solution described above and the doping density in the removed layer was calculated from the change in the Hall coefficient and sheet conductivity with each anodization step. Since we were not able to measure the exact amount of material removed by an anodization step, these measurements must be taken as approximate, but they serve to indicate the general shape of the profile.

We conjecture that the high short–circuit current seen on wafer #57–1 is due to the shallow junction and the steep decrease in doping from a very high value at the front surface. The low voltage is apparently due to a back contact problem; the results from the hybrid cells below show that low saturation current and high V_{oc} are not incompatible with this doping profile.

MOCVD

Likewise, in the case of epitaxial cells, the factor to which the cell performance is most sensitive was found to be the emitter thickness. Figure 3 compares the spectral response of epitaxial cells of three different emitter thicknesses and table 2 gives the corresponding cell performance. The dramatic improvement in current is apparent.

Attempts to make emitters thinner than 50 nm by straightforward MOCVD were not successful, but we were able to produce shallower junctions by beginning with a 100 nm emitter and thinning it by anodization. Figure 4 shows the increase in current we observed from this thinning.

The MOCVD process allows the doping levels to be controlled continuously, so we were able to investigate step– and graded–emitter structures, and to attempt to match the doping profiles of the successful implanted cells. Table 3 describes these cell structures briefly. The graded structures were processed into cells without thinning. Table 4 presents the results.

The spectral response curves of the step– and graded–emitter cells (figure 5) contain some interesting data. The two 100 nm graded emitters show relatively low blue response, indicating that they were not successful in providing improved collection of carriers generated at the surface, but the 30 nm graded emitter shows blue reponse surpassing that of the 18.8% implanted cell.

These results are very encouraging as they show that the necessary structures for a high–performance emitter can be grown in one step. After antireflection coating, the cells on wafer 241 achieved an open–circuit voltage of 882/mV, which is the highest yet achieved.

Hybrid Cells

As noted above, the implanted cells showed the highest short–circuit currents, and the epitaxial cells the highest open–circuit voltages. Accordingly, we undertook to combine the advantages of both structures by making cells with an epitaxial base and an implanted emitter.

MOCVD was used to grow a base layer without an emitter. The structure was the same as that used for the cells described in section 3, except that the final n–type layer was omitted. A piece of this wafer was then implanted with $3 \times 10^{18} m^{-2}$ ($3 \times 10^{14} cm^{-2}$) of silicon and annealed as

described above. Table 5 gives the Spire and NASA measurement results from this wafer, along with those from the 17.9% all–epitaxial wafer and those from a polished implanted wafer for comparison. It was this hybrid cell which achieved 18.8% efficiency in NASA measurements. Spectral response and I–V characteristics are shown in figures 6 and 7, respectively.

As can be seen from figures 6 and 7, the implanted emitter has better collection efficiency in the blue end of the spectrum than the thinned epitaxial emitter, and its saturation current is almost as low. We have found, as expected, that combining the epitaxial base with the implanted emitter yields a cell with the advantages of both: the high red response and high voltage of the epitaxial cells and the high blue response of the implanted cells.

Modeling

Theoretical modeling of the blue response was carried out in an attempt to estimate the emitter lifetime and the front surface recombination velocity.

A closed–form equation which describes the collection efficiency of a homogeneous emitter as a function of thickness, carrier lifetime and mobility, surface recombination velocity, and optical absorption length was derived. Cells of identical doping concentrations and different emitter thicknesses, ranging from 10 nm to 300 nm, were compared using the same equation.

Figure 8 compares the results with the theoretical model. The best fit resulted from a high surface recombination velocity of 1.5 to 1.8 $\times$ 10^5m/s, a hole mobility in the emitter of 70 to 100 cm^2/V s, and a high carrier lifetime in the emitter (0.1 ns). This value for surface recombination velocity is very close to the electron thermal velocity, which provides an upper limit on the SRV.

Although the agreement is not perfect, its persistence over more than a factor of ten in emitter thickness gives us confidence that surface recombination velocity is the limiting factor in the current collection. Models with lower recombination velocity required a shorter lifetime to fit the data from the thinner cells, and consequently they predicted a lower response than was observed for the thicker cells.

Finally, we attempted to use these modeling results to project the maximum efficiency for InP cells. The highest short–circuit current measured (from the hybrid implanted cells) was 360 A/m^2 (36.0 mA/cm^2) (NASA measurement). Although epitaxial cells have yielded lower currents (339 A/m^2 [33.9 mA/cm^2] was the highest), presumably the epitaxial cells could reach the same current, or slightly higher, with improved tailoring of the dopant profile. If this can be done while preserving the high V_{oc} (882 mV) and fill factor (84%) which we have seen in epitaxial cells, we would have an efficiency of 19.5% AM0. Although not yet achieved, this may be considered a realistic short–term goal.

Taking this as a baseline, there are two areas of improvement which we may consider. First, despite the considerable theoretical interest generated by InP, the parameters of the material are not well enough known to allow a definitive determination of the maximum achievable open–circuit voltage. V_{oc} of 1021 mV has been achieved with GaAs, [ref. 15] which has a very similar band structure, and so, in the absence of theoretical indications to the contrary, we may suppose that the achievable limit to the V_{oc} for InP is the same relative to the band–gap, or in the neighborhood of

950 mV. Our results indicate that the V_{oc} of the current cells is largely base–limited, and so efforts to increase V_{oc} must focus on improving the material quality toward the level achieved with GaAs.

The theoretical maximum AM0 current for indium phosphide is calculated to be 420 to 440 A/m^2 (42 to 44 mA/cm^2). It is clear that the largest part of the uncollected current in the current cells is in the blue end of the spectrum, and our results suggest that the surface recombination velocity is the cause. If this is true, then finding a way to passivate the front surface of these cells could be very important.

Table 6 shows our estimates of the efficiencies realizable under various conditions. By making certain assumptions about the surface recombination velocity, we can project that efficiencies over 20% will be possible with a lattice–matched window layer.

Radiation Effects

The radiation resistance of these cells was evaluated as well. Cells were irradiated with $5 \times 10^{19} m^{-2}$ ($5 \times 10^{15} cm^{-2}$) electrons at 1 MV, and then annealed, both thermally and by forward–bias current injection. The effects of the radiation and annealing were assessed by both cell performance measurements and deep level transient spectroscopy (DLTS). Table 7 gives the anneal conditions and results. Figure 9 shows that the most important mechanism of efficiency degradation is the loss of red response, which presumably is the result of a decrease in base carrier lifetime. The anneal seems to have recovered some of the radiation damage, but it is difficult to quantify since control cells which were not irradiated also improved during the anneal.

References

[1] A. Yamamoto, M. Yamaguchi, and C. Uemura, "High Conversion Efficiency and High Radiation Resistance InP Homojunction Solar Cells," Appl. Phys. Lett. **44**, 611 (1984).

[2] M. Yamaguchi, K. Ando, A. Yamamoto and C. Uemura, "Minority–Carrier Injection Annealing of Electron Irradiation–Induced Defects in InP Solar Cells," Appl. Phys. Lett. **44**, 432 (1984).

[3] M. Yamaguchi, Y. Ito, and K. Ando, "Room–Temperature Annealing of Radiation–Induced Defects in InP Solar Cells," Appl. Phys. Lett. **45**, 1206 (1984).

[4] A. Yamamoto, M. Yamaguchi, C. Uemura, "High Efficiency Homojunction InP Solar Cells," Appl. Phys. Lett. **47**, 975 (1985).

[5] I. Weinberg, C.K. Swartz, R.E. Hart and R.L. Statler, "Radiation and Temperature Effects in Gallium Arsenide, Indium Phosphide, and Silicon Solar Cells," *Rec. of the 19th IEEE Photovoltaic Specialists Conference*, New Orleands, May 1987, p. 548.

[6] M. Yamaguchi, Y. Ito, and C. Uemura, "22% Efficient and High Radiation–Resistant InP Solar Cells," *Proc. of the Second International Photovoltaic Science and Engineering Conf.* (Beijing) Aug. 1986.

[7] T. J. Coutts and S. Naseem, "High Efficiency Indium Tin Oxide/Indium Phosphide Solar Cells," Appl. Phys. Lett. **46**, 164 (1985).

[8] S. Bothra et al., "Characterization and Modeling of Open Tube Diffused N^+-P Bulk InP Solar Cells," *19th IEEE Photovolatic Specialists Conference*, May 1987.

[9] K. Y. Choi, C. C. Shen, and B. I. Miller, "P/N InP Homojunction Solar Cells by LPE and MOCVD Techniques," *19th IEEE Photovolatic Specialists Conference*, May 1987.

[10] M. B. Spitzer, C. J. Keavney, S. M. Vernon and V. E. Haven, "Indium Phosphide Shallow Homojunction Solar Cells Made by MOCVD," Appl. Phys. Lett. **51**, 364 (1987).

[11] M. Sugo, A. Yamamoto and M. Yamaguchi, "n+-p-p+ Structure InP Solar Cells Grown by Organometallic Vapor-Phase Epitaxy," IEEE Trans. ED-34, 772 (1987).

[12] C. J. Keavney and M. B. Spitzer, "Indium Phosphide Solar Cells Made by Ion Implantation," Appl. Phys. Lett. **52**, 1439 (1988).

[13] J. C. C. Fan, C. O. Bozler and R. L. Chapman, "Simplified Fabrication of GaAs Homojunction Solar Cells with Increased Conversion Efficiencies," Appl. Phys. Lett. **32**(6), 390 (1978).

[14] Y. Robach et al., "New Native Oxide of InP with Improved Electrical Interface Properties," Appl. Phys. Lett. **49**(19), 1281 (1986).

[15] S. P. Tobin et al., "A 23.7% Efficient One-sun GaAs Solar Cell," *Rec. of the 19th IEEE Photovoltaic Specialists Conference*, New Orleans, May 1987, p. 1492.

Table 1. Effect of Implant Energy on Cell Performance

Wafer Ion #	Implant Voltage (kV)	Avg. V_{oc} (mV)	Avg. J_{sc} (A/m^2)	Avg. FF	Avg. Eff. (%)	Highest Eff. (%)
57-1[ac] Si (4 cells)	5	614 (±11)	331.6 (± 1.7)	0.723 (±.038)	10.7 (±0.5)	11.2
42-2f Si (2 cells)	10	806 (± 1)	298.2 (± 1.3)	0.718 (±.061)	12.6 (±1.0)	13.3
42-3a[ab] Si (1 cell)	50	777	182.1	0.757	7.8	7.8

Measurements at Spire, Air mass 0 (1372 W/m^2), 298 K, silicon reference cell, with antireflection coating.

Notes: [a] Results estimated from measurements without antireflection coating.

[b] Results calculated from AM1.5 measurement.

[c] The low voltage is attributed to an incomplete back contact anneal.

Table 2. Performance of Epitaxial Cells.

Run #	Emitter Thickness (nm)	Avg. V_{oc} (mV)	Avg. J_{sc} (A/m^2)	Avg. FF	Avg. Eff. (%)	Highest Efficiency (%)
72 (6 cells)	20	855 (±3)	223.3 (±1.0)	0.828 (±.013)	11.5 (±0.2)	11.8
67 (3 cells)	100	850 (±16)	172.7 (±2.6)	0.807 (±.016)	8.8 (±0.2)	9.0
68 (3 cells)	300	850 (±4)	103.1 (±0.5)	0.814 (±.016)	5.3 (±0.1)	5.4

Measurements at Spire, Air mass 0 (1372 W/m^2), 298 K, silicon reference cell, no antireflection coating.

Table 3. Cell Structures Investigated by MOCVD

Run #	Thickness (nm)	Doping (m^{-3})	Purpose
233	50	1.5×10^{25}	Control
240	100	Two Step: 1.5×10^{23}- 1.5×10^{25}	High-low emitter structure to shield the lightly-doped layer from the surface
241	100	Graded 1.5×10^{23}- 1.5×10^{25}	To test the graded emitter structure
242	30	Graded 1.5×10^{23}- 3×10^{25}	To duplicate the implanted emitter

Table 4. Performance of Graded Epitaxial Cells.

Run #	Emitter Thickness (nm)	Avg. V_{oc} (mV)	Avg. J_{sc} (A/m^2)	Avg. FF	Avg. Eff. (%)	Highest Efficiency (%)
233b (4 cells)*	35 nm	814 (±15)	211.5 (±0.2)	0.777 (±.032)	9.8 (±0.6)	10.2
240 (8 cells)	100 nm	789 (±22)	206.0 (±1.3)	0.707 (±.017)	8.4 (±0.4)	9.0
241 (7 cells)*	100 nm	869 (±1)	208.0 (±1.0)	0.837 (±.003)	11.0 (±0.1)	11.1
242 (8 cells)	30 nm	768 (±50)	218.2 (±3.9)	0.645 (±.068)	7.9 (±1.1)	9.8

Measurements at Spire, Air mass 0 (1372 W/m^2), 298 K, silicon reference cell, no antireflection coating.

*On each of these two wafers, one cell, located near the edge of the wafer, had much lower efficiency. These cells have been omitted from the averages.

Table 5. Comparison of Best Cells.

Run #	Process	Measured at	Avg. V_{oc} (mV)	Avg. J_{sc} (A/m^2)	Avg. FF	Avg. Eff. (%)	Highest Efficiency (%)
4970 (6 cells)*	All-Epitaxial	Spire	865 (±2)	318.9 (±0.5)	0.830 (±.011)	16.7 (±0.3)	17.0
		NASA	864 (±2)	336.7 (±1.9)	0.826 (±.013)	17.5 (±0.4)	17.9
5021-2 (9 cells)*	Implanted	Spire	833 (±5)	340.8 (±0.5)	0.797 (±.014)	16.5 (±0.4)	17.0
5021-3 (8 cells)*	Hybrid	Spire	870 (±6)	349.5 (±1.4)	0.806 (±.015)	17.9 (±0.4)	18.2
		NASA	868 (±6)	356.7 (±1.7)	0.808 (±.016)	18.2 (±0.5)	18.8

Measurements at Spire, Air mass 0 (1372 W/m^2), 298 K, silicon reference cell, with antireflection coating.

*On each of these two wafers, one cell, located near the edge of the wafer, had much lower efficiency. These cells have been omitted from the averages.

Table 6. Projected InP Cell Efficiencies.

	V_{oc} (mV)	J_{sc} (A/m^2)	FF	Efficiency (%)
Present best cell (5021-3)	873	357	0.829	18.8
Non-ideal recombination reduced	882	357	0.850	19.5
Shadow loss reduced to 3% (larger cell)	882	364	0.850	19.9
Window layer added (surface recombination reduced to 10^3 m/s)	886	377	0.850	20.7
Bulk diffusion length increased to 15 um	933	379	0.855	22.0
Theoretical upper limit (no shadow, reflection, or series resistance)	950	427	0.878	26.0

Table 7. Effects of Irradiation and Annealing.
(Cell 248-8)

	H_4 Trap Density (m^{-3})	V_{oc} (mV)	J_{sc} (A/m^2)	FF	Eff. (%)
Initial	0	768	311.1	0.745	13.0
After irradiation (5×10^{19} m^{-2} Electrons @ 1 MV)	8.4×10^{18}	712	259.5	0.727	9.8
After thermal anneal 348K, 1800 s (75°C, 30 min)	1.7×10^{18}				
After thermal anneal 373 K, 1800 s (100°C, 30 min)	5.8×10^{17}				
After current anneal 270 KA/m^2, 90 s	9.2×10^{16}				
After thermal anneal 523K, 1800 s (250°C, 30 min)		730	283.6	0.732	11.0

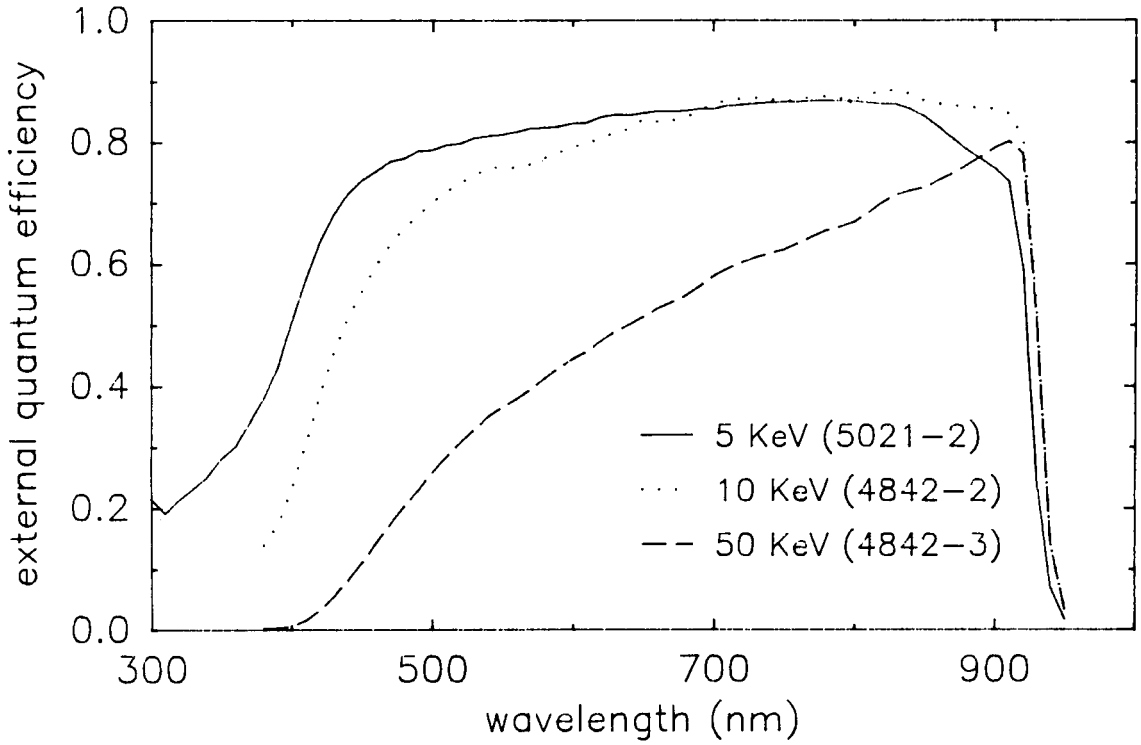

Figure 1. EFFECT OF IMPLANT ENERGY ON IMPLANTED InP CELLS. The lower voltages, which yield the shallower junctions, give improved blue response.

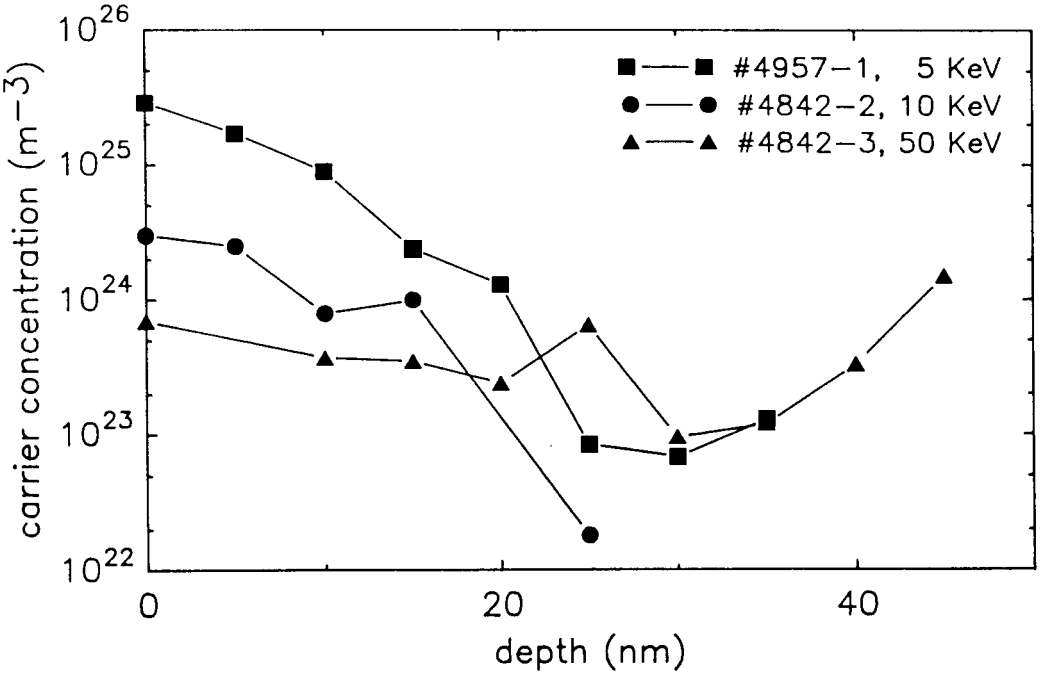

Figure 2. DOPING PROFILES OF JUNCTIONS FORMED IN InP BY ION IMPLANTATION OF SILICON. Differences in the processing apparently cause large differences in the overall doping levels, but the shallow, graded junction which results from the low-energy implant is apparent.

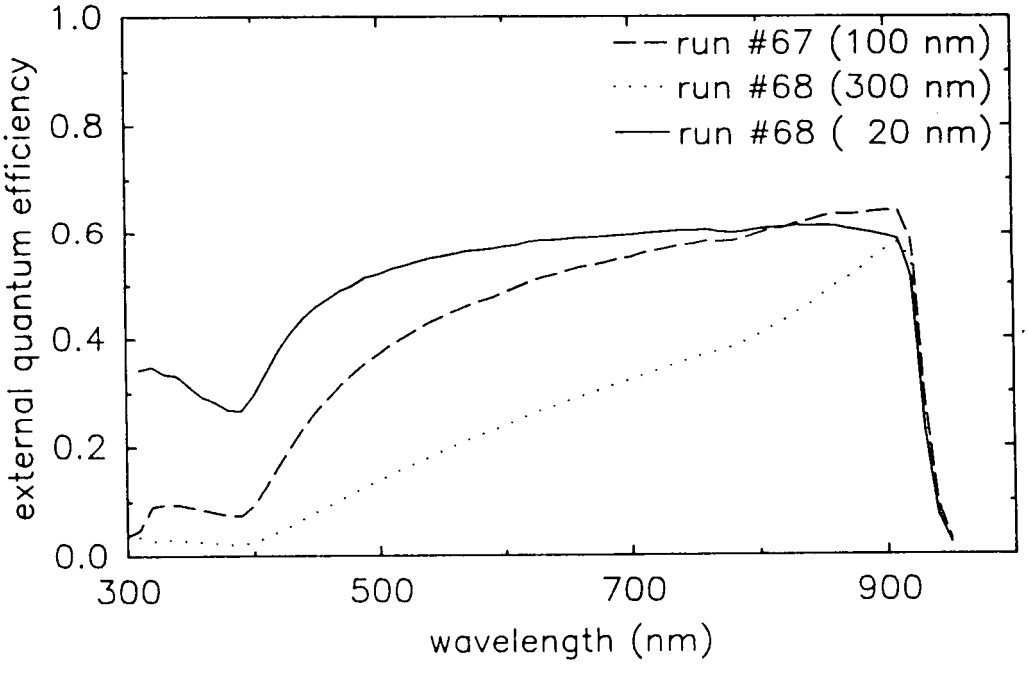

Figure 3. EFFECT OF EMITTER THICKNESS ON EPITAXIAL CELLS. (External quantum efficiency before antireflection coating is shown.) The cell with the 20 nm emitter was made by anodization.

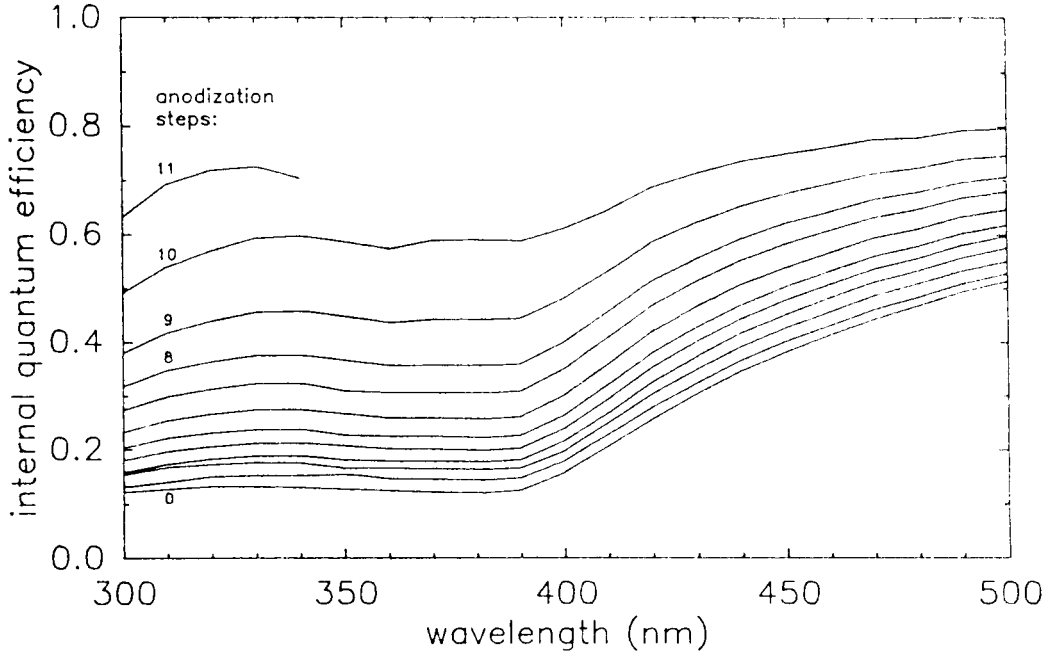

Figure 4. CHANGE IN THE QUANTUM EFFICIENCY WITH ANODIZATION OF AN EPITAXIAL CELL. Each anodization step removes approximately 10 nm from the front of the cell; since the cell failed after the eleventh step, the initial emitter thickness was apparently close to 110 nm.

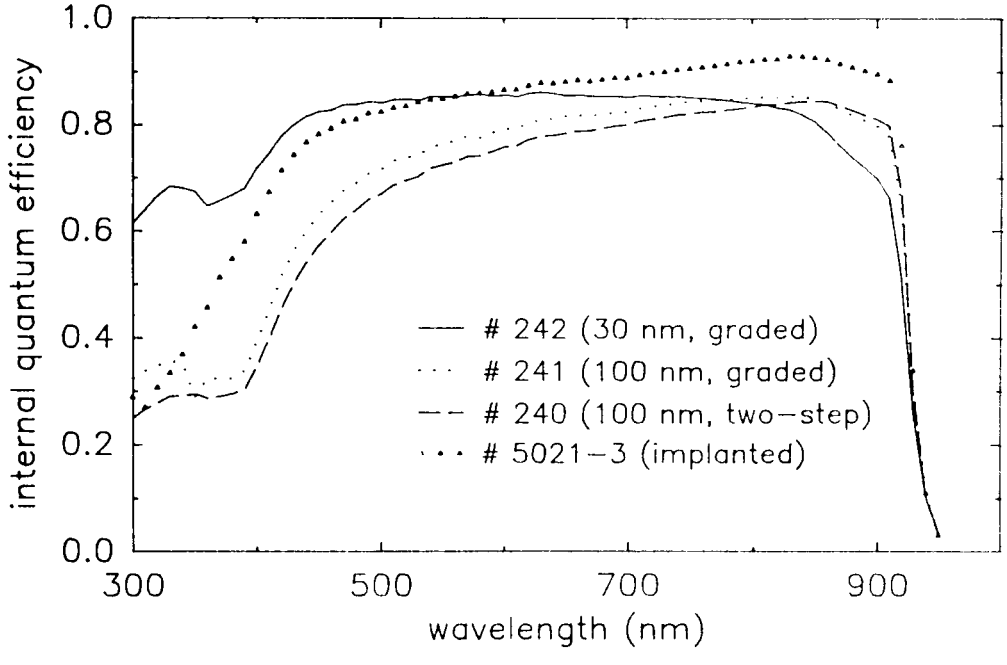

Figure 5. GRADED-DOPING EMITTERS, COMPARED TO THE IMPLANTED EMITTER OF THE 18.8% CELL. The thin graded structure has resulted in remarkable blue response.

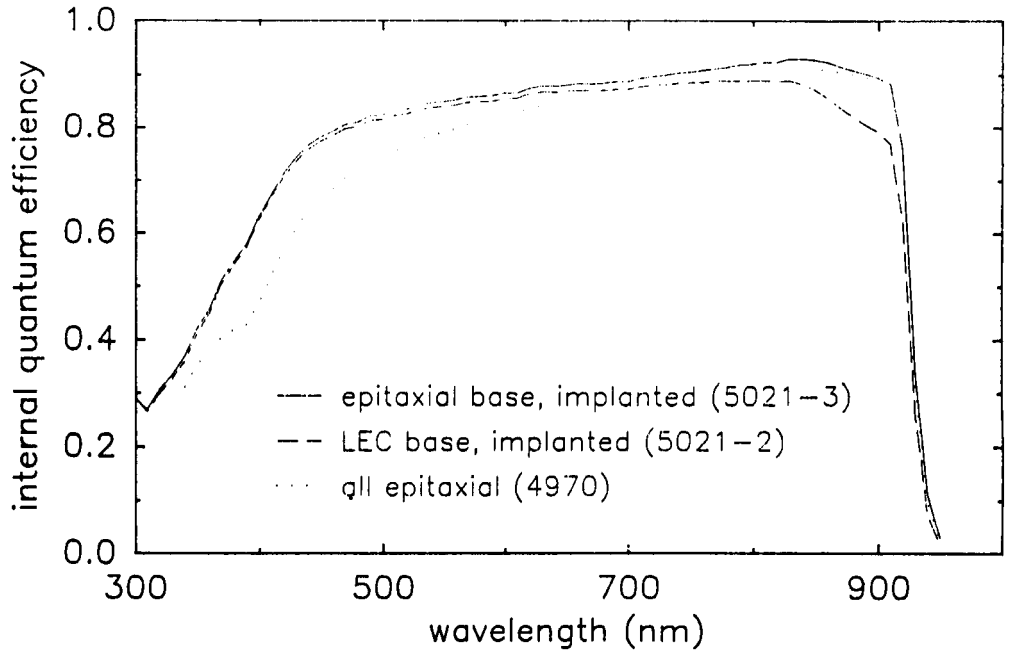

Figure 6. SPECTRAL RESPONSE CURVES OF THE IMPLANTED-EMITTER SOLAR CELLS, WITH AN EPITAXIAL CELL CURVE FOR COMPARISON. The curves show that the epitaxial base yields higher red response and the ion-implanted emitter yields higher blue response.

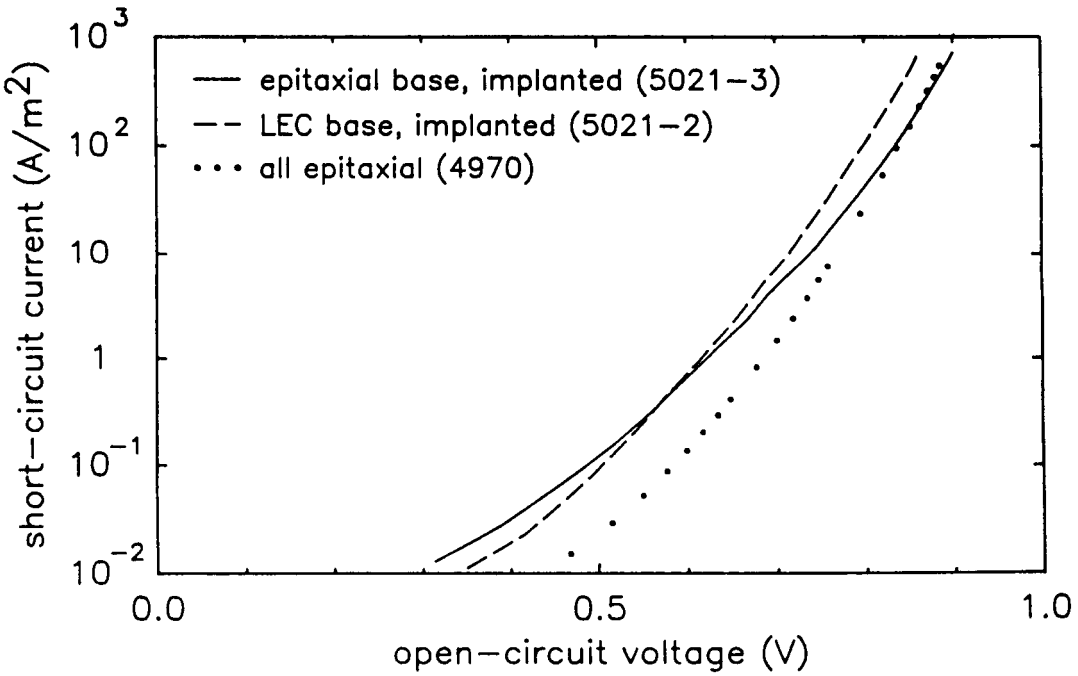

Figure 7. CURRENT-VOLTAGE CHARACTERISTICS OF THE IMPLANTED-EMITTER SOLAR CELLS, WITH AN EPITAXIAL CELL CURVE FOR COMPARISON.

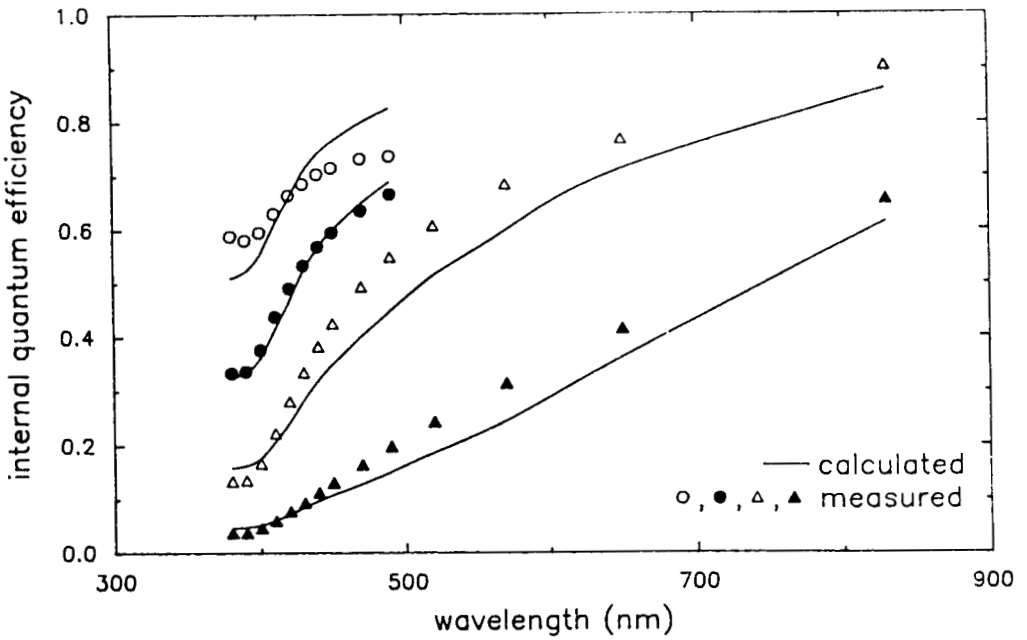

Figure 8. MODELING OF SPECTRAL RESPONSE OF THE THINNED EPITAXIAL CELLS. The estimated emitter thicknesses of these four cells (from top to bottom) were 11, 34, 110, and 300 nm. The thicknesses derived from the modeling are respectively 23, 42, 93, and 300 nm. As before, the modeling indicates that the low blue response is due to a high surface recombination velocity, rather than a low carrier lifetime.

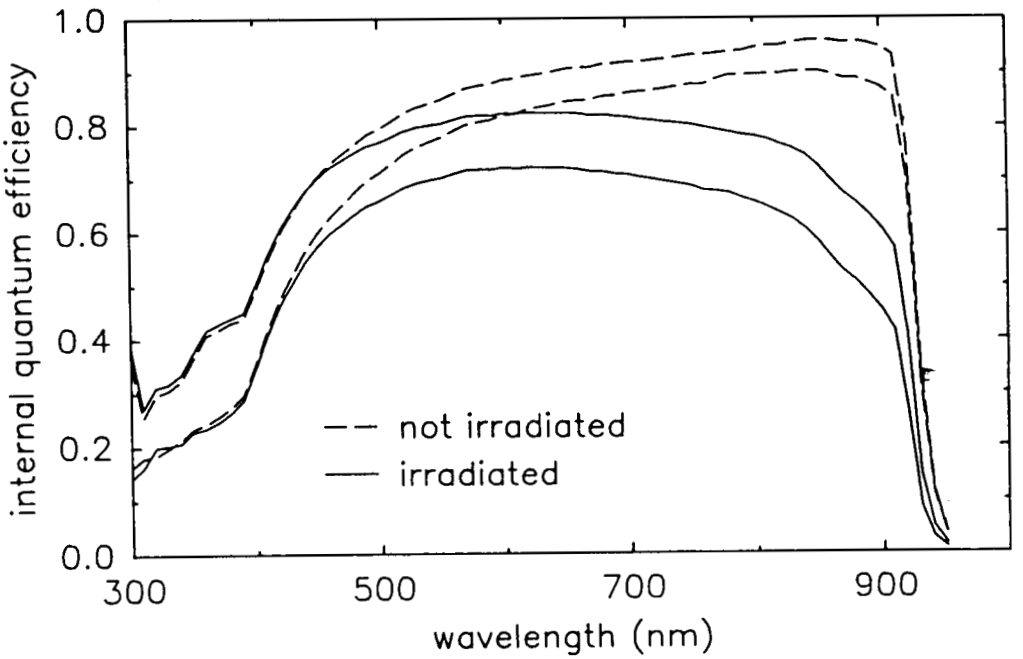

Figure 9. EFFECT OF ELECTRON IRRADIATION AND ANNEALING ON SPECTRAL RESPONSE OF AN EPITAXIAL SOLAR CELL. The primary mechanism of efficiency degradation is the loss of red response, which presumably is the result of a decrease in base carrier lifetime. The electron dose was 5×10^{19} m^{-2} (5×10^{15} cm^{-2}) at 1 MV. Two anneals were used: 348 K (75°C) and 373 K (100°C) for 1800 s (30 min) each. (The upper curve in each pair was measured after annealing.)